Technical Note

Landslides
DOI 10.1007/s10346-026-02694-0
Received: 3 August 2025
Accepted: 7 January 2026

Zhiang Chen · Emily C. Geyman · Michael P. Lamb

Rapid hazard prediction and assessment of post-fire debris flows using UAV lidar: Eaton Fire, California

Abstract Although post-wildfire debris flows pose significant hazards to property and life, robust prediction systems for the magnitude and timing of debris flows remain limited. This knowledge gap exists in part due to sparse data on historical debris-flow events. In response to the Eaton Fire, part of the broader 2025 Los Angeles Wildfire event, we deployed unpiloted aerial vehicle (UAV) lidar systems to map topographic change before and after significant rainfall events. We perform two types of analyses. First, through volumetric measurements of post-rainstorm sediment accumulation in 14 debris basins, we quantify the volumes of debris flows mobilized during a major post-fire rainstorm. Second, using UAV lidar surveys acquired before the first major rainfall, we measure the volume of sediment mobilized as dry ravel during the wildfire. We compare the pre- and post-rainstorm surveys to evaluate whether the debris flows were sourced predominantly from dry-ravel cones filling the channel network. We show that measuring the dry-ravel volumes provides a data-driven approach to predicting hazards. By integrating the UAV lidar with field observations, time-lapse cameras, rainfall monitoring, and airborne lidar, we present a framework for capturing the spatial and temporal dynamics of debris flows. Finally, we discuss logistical challenges related to airspace access and weather constraints, and offer recommendations for integrating UAV lidar into routine postfire hazard mitigation workflows. This study underscores the transformative potential of UAV lidar monitoring for improving postfire debris-flow hazard prediction, emergency response, and long-term planning.

Keywords Debris flows · UAV lidar · Hazard assessment · Hazard prediction · Los Angeles Wildfire · Topographic change detection

Introduction

Post-wildfire debris flows pose substantial risks to life and property (Cannon et al. 2003; Cannon and DeGraff 2009). Accurate prediction of debris-flow hazards remains challenging because debris flows depend on a blend of factors spanning from the local topography (terrain steepness), the landscape history (the time since last burn and sediment availability), the burn severity (soil properties and vegetation loss), and the external forcing (rainfall duration and intensity) (Staley et al. 2017; Nikolopoulos et al. 2015; Gartner et al. 2014; DiBiase and Lamb 2013). Empirical models calibrated using historical events require updating to reflect evolving conditions, such as reduced sediment availability following frequent fire-flood cycles (Gartner et al. 2014; Rengers et al. 2024). These challenges highlight the urgent need for both improved predictive models that account for evolving postfire conditions and enhanced assessment techniques that leverage rapid, high-resolution data to monitor sediment mobilization.

The current operational hazard assessments for post-fire debris flows in the American West primarily rely on empirical models developed by the U.S. Geological Survey (U.S. Geological Survey 2018), which estimate debris-flow likelihood and volume based on historical occurrence and magnitude data, rainfall storm conditions, terrain and soils information, and burn-severity data (Staley et al. 2016; Gartner et al. 2014). Although widely used for emergency planning, these models still present substantial opportunities for improvement. First, the paucity of storm-scale data hampers efforts to rigorously validate and refine model predictions. Volume measurements accumulated across multiple storm events obscure the relationship between individual storms and sediment delivery. Thus, storm-scale monitoring of debris volumes (such as those captured in engineered debris basins) after each storm event can help refine empirical models. Second, storm-scale monitoring of debris basin capacities is essential for hazard assessment. As sediment accumulates, basins rapidly lose their ability to capture additional material during subsequent storms. Although sediment yield predictions provide useful context, decision-makers also need updated estimates of remaining storage before the next event, which may occur within days or weeks. Because storm intervals are often too short to clear every basin, agencies must prioritize which ones to empty.

Additionally, recent studies suggest that a substantial portion of the sediment that fuels post-wildfire debris flows in steep terrain is initially mobilized as dry ravel during or immediately following the fire (DiBiase and Lamb 2013; Lamb et al. 2011; DiBiase and Lamb 2020; Palucis et al. 2021; Gabet 2003; Florsheim et al. 1991). The incineration of vegetation dams on steep hillslopes releases previously trapped soil and sediment, which then bounce and roll downslope under the force of gravity (Lamb et al. 2011). This process delivers loose material into channel beds, forming ravel cones (Ramirez et al. 2024; Peduto et al. 2022), even before any rainfall (Lamb et al. 2013; DiBiase and Lamb 2013). Thus, quantifying the volume of this mobilized sediment post-wildfire–but pre-rainfall–offers a pathway to create data-driven predictive hazard assessments, allowing agencies to prepare for or mitigate debris-flow impacts (DiBiase and Lamb 2020).

Multiple remote sensing techniques have been employed to quantify sediment dynamics after wildfire, each with trade-offs in resolution, spatial coverage, and operational feasibility. Early efforts to quantify postfire sediment transport relied on terrestrial laser scanning lidar surveys of hillslopes (Staley et al. 2014; Rengers et al. 2021). These scans captured high-resolution topography but

were constrained in spatial coverage. To expand coverage, researchers applied UAV photogrammetry, which offered improved spatial reach and flexible deployment (Palucis et al. 2021). However, UAV photogrammetry often lacked accuracy and vegetation penetration capability. To map broader terrain, other studies turned to airborne lidar (DiBiase and Lamb 2020; Scheidl et al. 2008). Early attempts, however, had overlapping lidar only in certain areas given the sparsity of historic lidar, and uncertainty stemming from coarse resolution did not allow the sediment budget to be closed (DiBiase and Lamb 2020). UAV lidar has emerged as a promising intermediate approach that addresses many limitations of prior methods. These systems offer high-resolution, high-accuracy topographic data with the added benefits of rapid deployment and storm-scale repeatability. Although UAV lidar remains limited in spatial extent compared to airborne platforms, it is ideally suited for targeted monitoring of high-risk basins and catchments, providing an agile and cost-effective tool for capturing the topographic change to advance debris-flow prediction and early-warning capabilities.

We present a UAV lidar-based approach for rapid hazard prediction and assessment of postfire debris flows, using the Eaton Fire (part of the 2025 Los Angeles Wildfire event) as a case study. The Eaton Fire ignited on 7 January 2025 in the San Gabriel Mountains of Los Angeles County and burned approximately 14,000 acres (Los Angeles County Coordinated Joint Information Center 2025). Its proximity to (and destruction of) urban neighborhoods highlighted the urgent need for timely assessment of the remaining hazards (such as debris flows) that would persist for the weeks, months, and years after the fire had been contained (Graber et al. 2023). In the weeks following containment, a series of storms impacted the burn area, including a major event on February 13–14 that triggered significant debris flows in almost every catchment in the burned area. These conditions provided a critical testbed for our approach, which utilized UAV lidar surveys to (i) estimate postfire dry-ravel sediment loading in upstream channels prior to rainfall, and (ii) measure debris deposition in basins at storm-scale intervals, enabling both predictive and responsive hazard assessment. Overall, we aim to show that rapid UAV lidar monitoring represents a transformative tool for improving the accuracy, timeliness, and effectiveness of postfire debris-flow hazard prediction and mitigation.

Study area

The San Gabriel Mountains (SGM), located north of Los Angeles, are an ideal natural laboratory for studying wildfire-induced sediment transport and debris flows (Eaton 1936; Heimsath et al. 2012; Krammes 1965; DiBiase and Lamb 2013). The steep topography of SGM promotes dry ravel by gravitationally delivering sediment to channels after wildfire (DiBiase and Lamb 2013), enabling rapid channel loading. This preconditioning lowers the rainfall threshold for debris-flow initiation, especially in narrow headwater valleys with slopes exceeding 30° (DiBiase and Lamb 2020; Prancevic et al. 2014; Palucis et al. 2021). The dense chaparral vegetation in the SGM traps sediment on steep hillslopes during inter-fire periods, forming vegetation dams. Following a wildfire, the incineration of these dams releases large volumes of stored material downslope via dry ravel (Lamb et al. 2011, 2013; Rice 1982; Hubbert et al. 2012). To mitigate downstream hazards, Los Angeles County has constructed and actively maintains a network of debris basins at canyon mouths throughout the range (Los Angeles County Department of Public Works 2021). Debris basins offer a unique opportunity to study debris flows in this region because, when overflow does not occur, the deposited material remains fully contained, and its total volume can be measured.

Following the Eaton Fire, we conducted UAV lidar surveys across multiple affected catchments before and after the major storm events. Figure 1 provides the spatial context of the Eaton Fire, with the locations and names of 14 surveyed debris basins. In this paper, we focus in particular on the Bailey catchments, which contribute flow and sediment to five debris basins: Carriage House, Sunnyside, Bailey, Auburn, and Carter.

Methods

UAV lidar data collection

To capture high-resolution topographic data following the Eaton Fire, we conducted multiple surveys using a UAV lidar-based mapping system. Figure 2 illustrates the UAV lidar system in both its packed and operational configurations. We deployed a DJI Matrice 350 RTK platform equipped with a DJI Zenmuse L2 lidar sensor. For RTK GPS correction, we used Emlid Reach RS3, a multi-band GNSS receiver. A portable power generator was used to power the battery station, charging four pairs of UAV batteries in the field.

We conducted UAV surveys at an altitude of 100–120 m above ground level, utilizing the terrain-following feature to maintain a consistent ground sampling resolution. We set an 80% front overlap and a 20% lateral overlap between data frames. The UAV operated at a maximum speed of 15 m/s, with an average flight speed of 6 m/s. This flight configuration resulted in a point density of 500–700 points/m^2 in point clouds and a 2–3.5 cm/pixel resolution in orthomosaics, while maintaining an overall elevation accuracy (root-mean-square error) of 2–3 cm over bare ground surfaces. Additionally, RGB image collection during surveys was enabled to colorize the point clouds.

This UAV lidar-based mapping system enabled rapid deployment and efficient data collection across multiple post-fire and post-storm study sites. Table 1 summarizes our UAV surveys conducted at the debris basins and Bailey catchments. For pre-fire topographic data, we used airborne lidar data from the U.S. Geological Survey (2023), which meets quality level 2 specifications, with a vertical root-mean-square error (RMSE) of ≤ 10 cm (U.S. Geological Survey 2020). Considering the typical point cloud coregistration uncertainty of 5 cm in sparsely vegetated and sloped regions (Lague et al. 2013), the minimum limit of detection at 95% confidence (minLOD_{95}) between the airborne and UAV lidar is 0.30 m, and the minLOD_{95} between two UAV lidar datasets is 0.17 m. These estimates follow the approach of Lague et al. (2013), assuming that each pixel contains only one independent vertical observation.

Point cloud processing

We applied two Post-Processing Kinematic (PPK) methods to process the UAV lidar data using DJI Terra. First, we used two nearby stations–both within 16 km of the field surveys–from the NOAA Continuously Operating Reference Station (CORS) Network as base stations for PPK correction of the UAV lidar data. Occasionally,

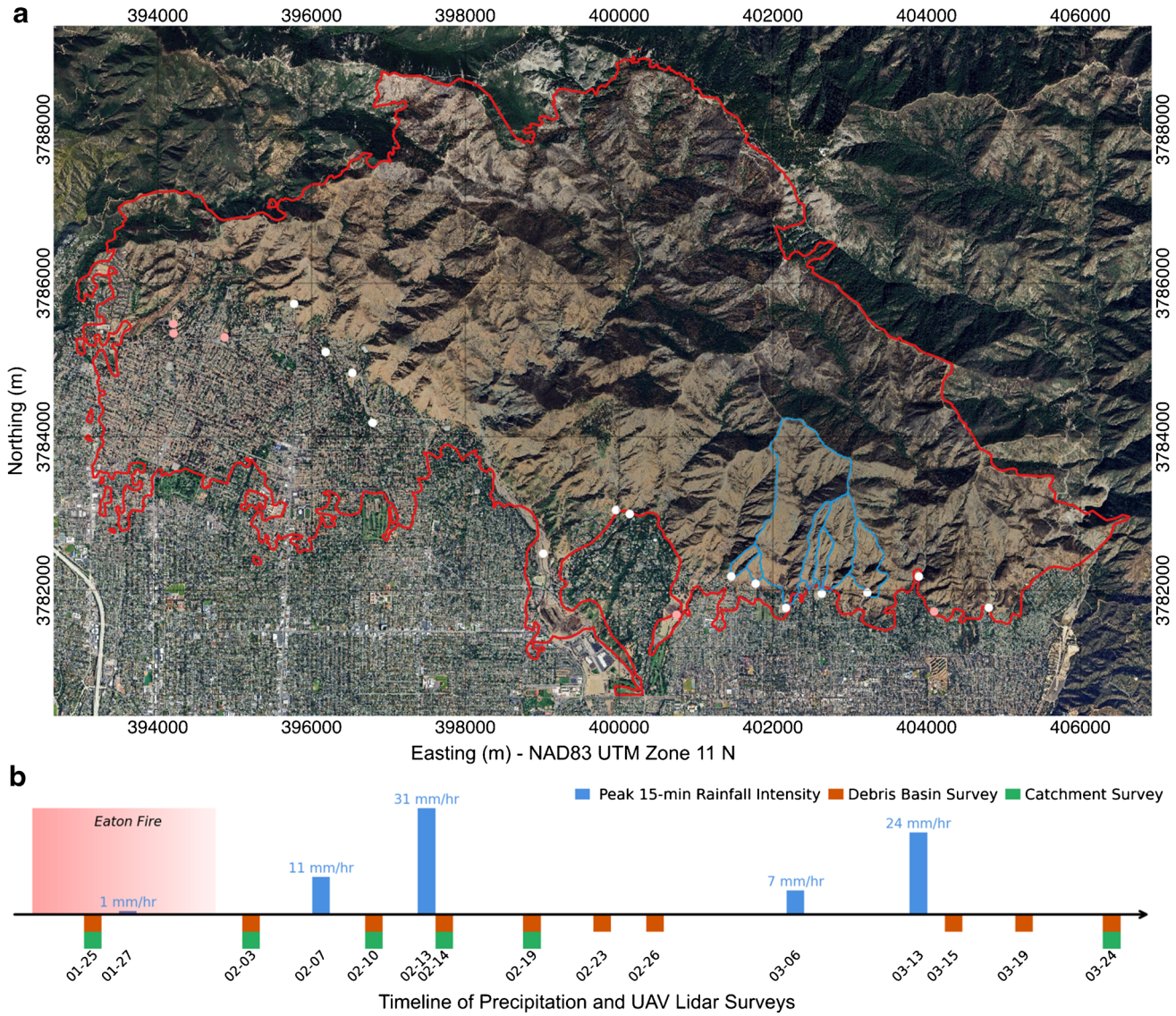

Fig. 1 **a** Study area and **b** timeline of precipitation and UAV lidar surveys. Eaton Fire perimeter (red outline) with survey areas of Los Angeles County debris basins and Bailey catchments (blue outline). Circles represent debris basin locations, scaled by design capacity. Numbered labels indicate the following basins: (1) Devonwood, (2) Las Flores, (3) Rubio, (4) Gooseberry, (5) Eaton Wash, (6) Kinneloa West, (7) Kinneloa East, (8) Carriage House, (9) Sunnyside, (10) Bailey, (11) Auburn, (12) Carter, (13) Sierra Madre Dam, and (14) Lannan. The GPS coordinates of these debris basins are included in Appendix Table 3. In **b**, precipitation data represent the peak 15-min rainfall intensity in *mm/hr* from LA County's network of ALERT tipping-bucket rain gauges (Los Angeles County Department of Public Works 2025). The Eaton Fire was fully contained on January 31, 2025, with the eastern portion extinguished by January 24

because of the long baseline length and lower sampling interval of CORS stations, the position and orientation solution (POS) did not consistently achieve 100% fixed solution along the entire flight trajectories. In this case, we first applied PPK using the CORS stations to correct the coordinates of the Emlid RS3 base station, which was set up much closer to the survey areas (with a maximum baseline of 2 *km*) and offered a higher sampling rate. The corrected base stations were then used to perform a second round PPK for the UAV lidar data, ensuring a 100% fixed POS throughout the entire flight trajectories. While we used RTK for real-time UAV navigation during surveys, for point cloud reconstruction, we applied PPK because of its higher positional accuracy and robustness to signal interruptions. Compared to RTK, which estimates position instantaneously, PPK incorporates both forward and backward filtering to refine the trajectory solution post-flight, ensuring sub-decimeter accuracy even when real-time corrections were intermittent.

After the PPK lidar reconstruction, we processed the point clouds to extract terrain surfaces and quantify elevation change, following airborne lidar processing protocols as recommended in the USGS report (Murchek et al. 2025) and previous studies (e.g., (Chen et al. 2017). Ground classification was performed using the Simple Morphological Filter implemented in PDAL (Pingel et al.

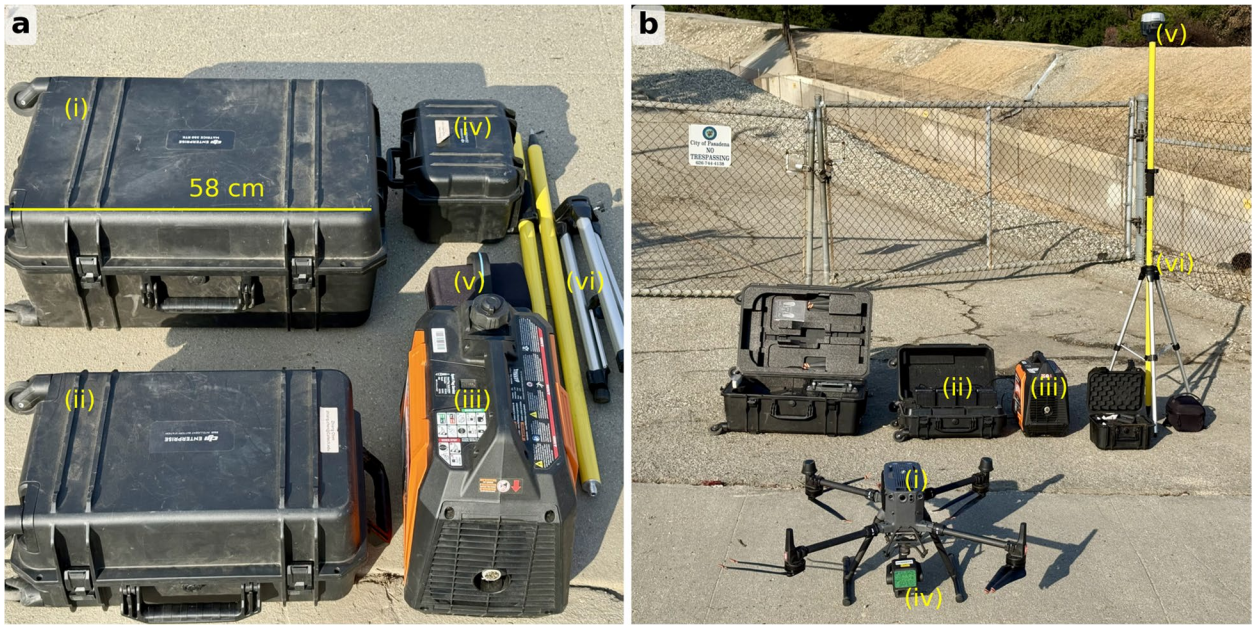

Fig. 2 UAV lidar mapping equipment in **a** packed and **a** setup configurations. Components include: (i) DJI Matrice 300 RTK UAV, (ii) battery station, (iii) portable generator for charging, (iv) DJI Zenmuse L2 lidar, (v) Emlid RS3 RTK GNSS base station, and (vi) base station tripod and pole. **a** The system packed for transport, while **b** the same equipment unpacked and ready for field operation

Table 1 UAV lidar surveys following the Eaton Fire

Location	01/25	02/03	02/10	02/14	02/19	02/23	02/26	03/15	03/19	03/24
Auburn	x	x	x	x	x	x	x	x	x	x
Bailey	x	x	x	x	x	x	x	x	x	x
Carriage house			x	x	x	x	x	x	x	x
Carter	x	x	x	x	x	x	x	x	x	x
Eaton wash						x	x	x	x	
Devonwood					x	x	x	x	x	
Gooseberry					x	x	x	x	x	
Kinneloa East						x	x	x	x	
Kinneloa West						x	x	x	x	
Rubio						x	x	x	x	
Lannan						x	x	x	x	
Las flores					x	x	x	x	x	
Sierra Madre Dam					x	x	x	x	x	
Sunnyside			x	x	x	x	x	x	x	x
Bailey catchments	x*	x	x	x*	x					x

The table includes coverage of 14 debris basins and 5 Bailey catchments. *UAV mapping covered partial Bailey catchments due to severe windy or cloudy conditions on January 25 and February 14, 2025

2013; Butler et al. 2021). Following vegetation removal, we aligned the ground-classified point clouds using iterative closest point (ICP) algorithms for spatial coregistration (Besl and McKay 1992; Lague et al. 2013). From the aligned point clouds, we generated preliminary digital elevation models (DEMs) by projecting points onto a horizontal raster grid and interpolating elevations using the inverse distance weighting (IDW) method (Shepard 1968). However, IDW interpolation did not fill all gaps in areas where lidar returns were sparse, particularly beneath dense vegetation. To address this, following standard airborne lidar workflows, we constructed a triangulated irregular network (TIN) surface by connecting ground points into non-overlapping triangles based on spatial proximity and topology (Peucker and Douglas 1975). DEMs were then generated by projecting elevation values from the TIN surface. Both IDW- and TIN-based DEMs serve complementary roles: the IDW DEMs offer higher density and fewer interpolation artifacts within debris basins, while the TIN DEMs provide more complete coverage in catchment areas where lidar returns are limited. Accordingly, we used IDW DEMs for debris basin analysis and TIN DEMs for catchment analysis. Figure 3 illustrates each step in the processing sequence from point cloud reconstruction to IDW DEM change detection.

We calculated sediment delivery to debris basins through topographic differencing of the post-storm (filled) debris basins to the pre-storm (unfilled) baseline. Airborne lidar data acquired on January 20–21, 2025, provided the baseline geometry of each basin prior to the storm (NV5 et al. 2025). Immediately following debris-flow deposition, clogging of the centrally located outlet tower in each debris basin led to partial ponding of surface water. To estimate the dry sediment yield in each debris basin, we performed repeat UAV surveys over the two weeks following the storm and observed an asymptotic decline in volume associated with water drainage. We quantified sediment deposition in 14 monitored debris basins in Table 1 using the UAV lidar surveys conducted on February 23, when all debris basins had been drained of their excess water. Six debris basins had material cleared after the acquisition of the post-fire airborne lidar on January 20–21, but prior to the debris-flow-producing rainstorm on February 13: Auburn, Devonwood, Kinneloa East, Lannan, Rubio, and Sierra Madre Dam. The removed material was measured and reported by the Los Angeles County Department of Public Works. We added the removed material to our observed volume changes (pre-storm to post-storm) to calculate the total deposition associated with the February 13 storm event. We then calculated the sediment yield as a percentage of the total

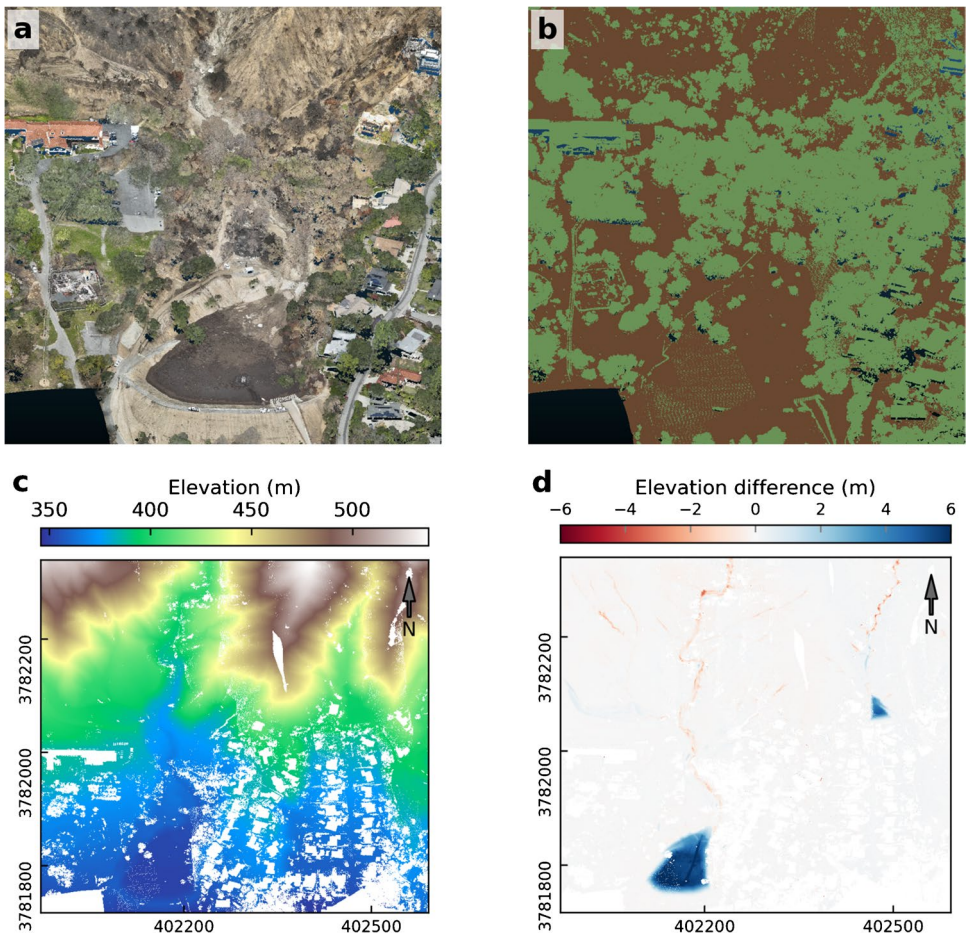

Fig. 3 Example of UAV lidar data processing steps. **a** Colorized point cloud reconstruction of Bailey Canyon from February 19, 2025. **b** Ground classification result. **c** Digital elevation model (DEM) generated from classified ground points. **d** DEM differencing map showing elevation changes between February 10 and February 19, 2025, following coregistration

debris basin capacity using the publicly available capacity data (Los Angeles County Department of Public Works 2021).

Previous studies have suggested that, in steep, bedrock-dominated landscapes such as SGM, the sediment fueling postfire debris flows is primarily sourced from dry-ravel cones, which fill the channel networks during the fire (Lamb et al. 2011; DiBiase and Lamb 2013, 2020). If validated, this relationship provides a powerful tool that allows one to measure the potential hazard directly from the landscape immediately after the fire and before rainfall. To examine this hypothesis, we conducted UAV lidar surveys in the Bailey catchments (Fig. 1) both after the fire (but before rainfall) and after the major February 13 rainstorm. To quantify the dry sediment mobilization during the fire, we used airborne lidar data acquired in 2023 (U.S. Geological Survey 2023) as the pre-fire baseline. We conducted UAV lidar surveys on February 10 (post-fire, pre-storm) and February 19 (post-storm) to focus on the debris flows triggered by the major February 13 storm event. (A minor rainfall on January 27 did not initiate debris flows and was therefore considered negligible for DEM differencing). We calculated postfire dry-ravel sediment accumulation by differencing the co-registered February 10 UAV DEM against the 2023 airborne DEM. Post-storm sediment removal during the storm was estimated by differencing the February 19 and February 10 UAV DEMs. We only calculated the postfire sediment loading and post-storm sediment removal within channel-network zones. The channel networks were calculated by sequential Fill Sinks (Wang and Liu 2006), Flow Accumulation (Freeman 1991), and Channel Network Extraction (Tarboton et al. 1991) in QGIS SAGA Hydrologic Terrain Analysis tools (Conrad et al. 2015). To define the analysis zones, we buffered the channel networks by 5 m on each side, resulting in an effective channel width of 10 m.

Other data

Other data used in our study includes time-sequenced photos from fixed cameras at the debris basins (ALERTCalifornia 2025), precipitation data (Los Angeles County Department of Public Works 2025), and USGS debris-flow volume predictions (U.S. Geological Survey 2025). For example, Fig. 4 presents photographs captured at key moments during the storm on February 13, 2025, illustrating the progressive accumulation of water and sediment in the Bailey debris basin. We calculated precipitation rates (*mm/hr*) using data from LA County's network of ALERT tipping-bucket rain gauges (Los Angeles County Department of Public Works 2025). Figure 5 displays the 15-min rain rate time series from two gauges, Eaton Wash Dam and Santa Anita Dam, located near the Bailey debris basin.

Fig. 4 Time-sequenced photos from a fixed camera at the Bailey debris basin capturing key stages of the storm event. Camera data from UC San Diego's ALERTCalifornia network (ALERTCalifornia 2025)

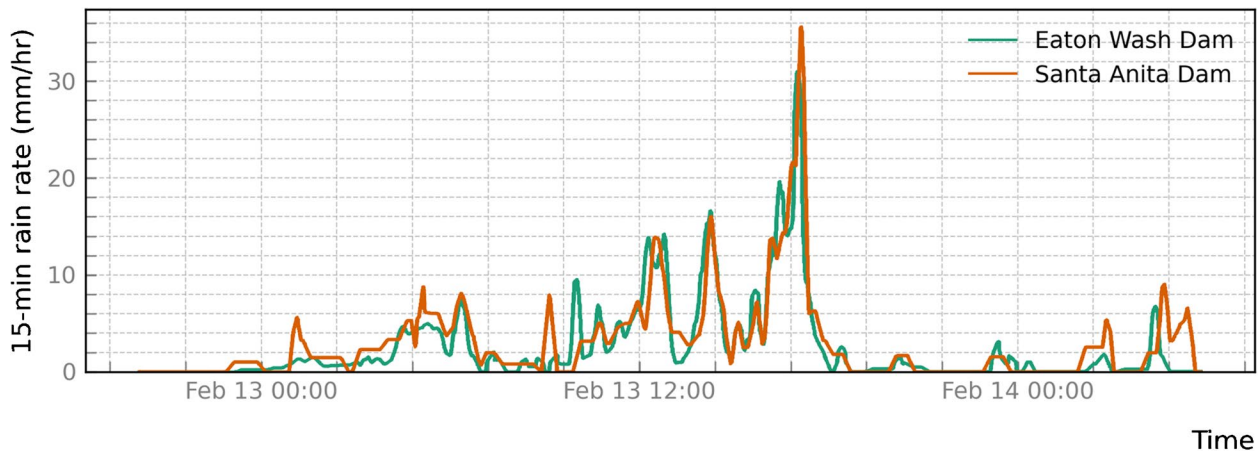

Fig. 5 Moving-window 15-min rain rates from February 13 to 14, 2025. Eaton Wash Dam and Santa Anita Dam are two rainfall measurement stations located near the Bailey catchments. Precipitation data from LA County's network of ALERT tipping-bucket rain gauges (Los Angeles County Department of Public Works 2025)

Based on the rainfall data along with other data such as historical debris-flow occurrence and magnitude data, terrain and soil properties, and burn-severity data from recently burned areas, USGS uses a multiple-linear-regression model to estimate the debris-flow volumes at the basin outlet from the upstream drainage network (Gartner et al. 2014). The model estimates the potential debris-flow volume in m^3 as:

$$\ln(V) = 4.22 + 0.13\sqrt{\text{ElevRange}} + 0.36\ln(\text{HM}) + 0.39\sqrt{I_{15}} \quad (1)$$

where ElevRange represents the elevation range within the upstream watershed in m, HM denotes the upstream area burned at high or moderate severity in km^2, and I_{15} is the spatially averaged peak 15-min rainfall intensity across the watershed in mm/hr. For example, based on the rainfall data from two nearby measurement stations (Fig. 5), I_{15} was selected as 32 mm/hr for the USGS-predicted debris-flow volumes. The prediction data is available at the USGS postfire debris-flow hazard assessment website (U.S. Geological Survey 2025).

Results

Measuring sediment yield in debris basins

By computing volumetric changes through DEM differencing, we measured sediment deposited in debris basins during the February 13–14 storm event. Immediately following the February 13 storm event, debris basins contained a mixture of sediment and ponded water, obscuring the total volume of deposited sediment. An example from the Bailey debris basin is shown in Fig. 6. As surface water drained over subsequent days, the basin contents transitioned to predominantly consolidated sediment, allowing for more robust sediment yield assessments. Between February 14 and 19, the average reduction in basin volume was 13.8% of the initially deposited material, and the additional reduction from February 19 to 23 was 2.3% (Fig. 7). These reductions indicate that volume estimates made immediately after the February 14 storm likely overestimated sediment deposition by approximately 15% because of ponded water in the debris basins.

We summarize the volume changes of the 14 UAV-surveyed debris basins following the Eaton Fire in Table 2. Figure 8 shows the estimated debris volumes deposited from the February 13 storm event, expressing the depositional volumes as a percentage of each basin's design capacity. This percentage reflects the loss in design capacity caused by the filled material. Design capacities were obtained from the Hydrologic Report of Los Angeles County Department of Public Works (2021). Although the reported percentages did not exceed 60%, field surveys documented minor overspill in multiple debris basins, including Sunnyside and Sierra Madre Dam. This discrepancy arises because the nominal capacities reported by Los Angeles County include the volumes of upstream depositional cones that extend beyond the basin spillway (Los Angeles County Department of Public Works 2021). Thus, when a debris basin reaches its design capacity, substantial sediment discharge beyond the spillway into downstream residential areas may have already occurred.

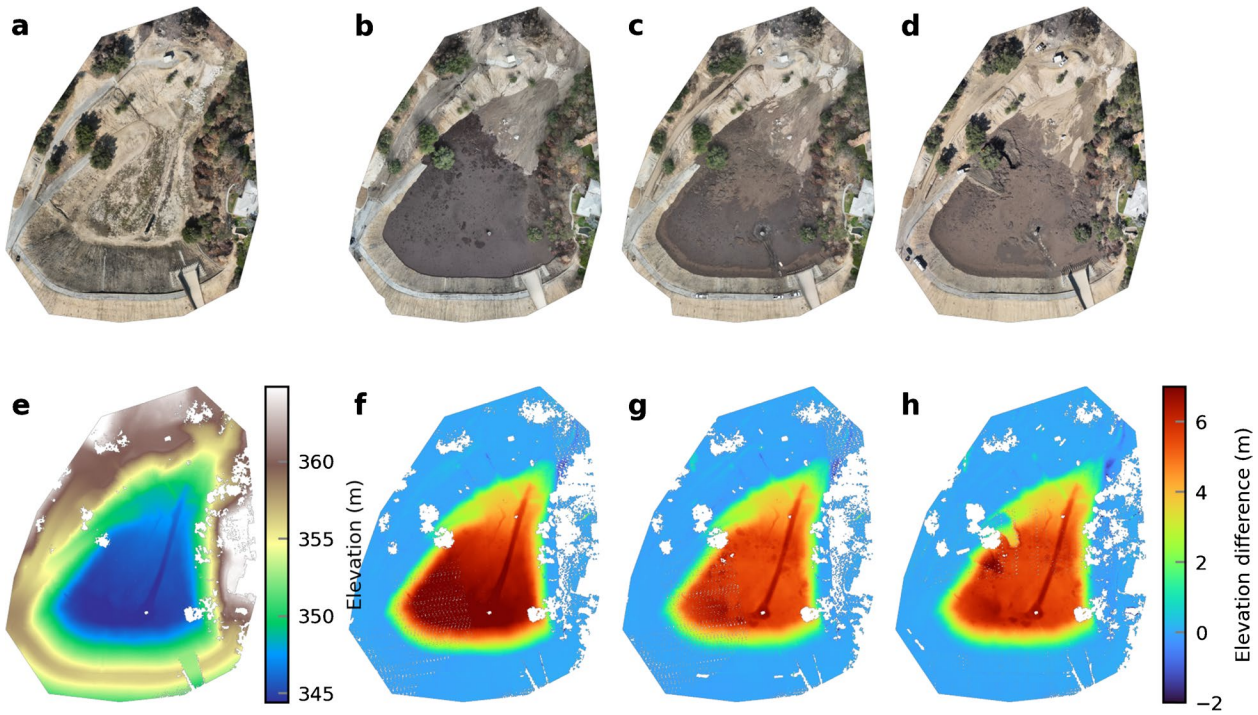

Fig. 6 UAV lidar surveys and volume changes in the Bailey debris basin. A major storm on February 13 triggered debris flows. We conducted UAV lidar surveys before and after the storm event. **a**–**d** Orthomosaics from UAV lidar surveys conducted on February 10, 14, 19, and 23, 2025. **e** DEM from the pre-storm UAV lidar survey on February 10, used as the baseline. **f**–**h** DEM differencing results from the February 14, 19, and 23 surveys relative to the baseline, illustrating temporal sediment volume changes primarily driven by the drainage of ponded water

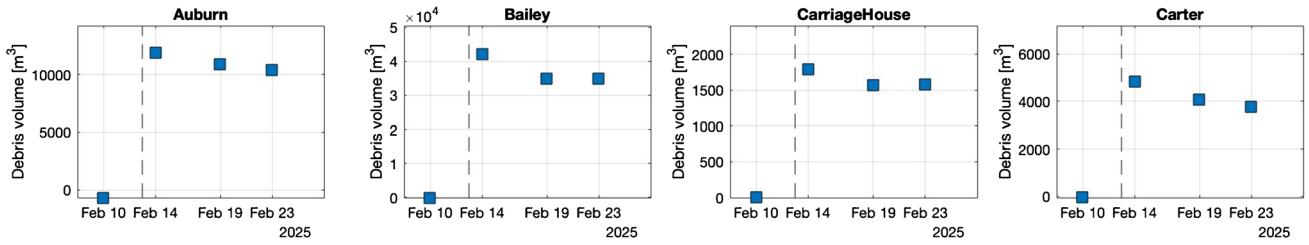

Fig. 7 Post-storm volume changes for four debris basins at the Bailey catchments. Airborne lidar acquired on January 20–21, 2025, served as the baseline for the pre-storm basin geometry (NV5 et al. 2025). We measured debris volumes from UAV lidar surveys conducted on February 10, 14, 19, and 23. The vertical dashed line denotes the peak rainfall intensity during the February 13 storm event. The measured volumes of material (sediment and water) in the debris basins declined by 15% in the 10 days following the storm event due to drainage of the excess water. Negative debris volume at Auburn on February 10 reflects preventive material removal by Los Angeles County Department of Public Works in preparation for the February 13 rainstorm

Table 2 Summary of debris basin volume change measurement

Debris Basin	Observed volume change (m^3)	Excavated volume (m^3)	Deposited volume (m^3)	Design capacity (m^3)	% of design capacity loss
Auburn	10,372	772	11,144	28,831	39
Bailey	34,815	0	34,815	98,457	35
Carriage House	1578	0	1578	10,168	16
Carter	3777	0	3777	21,178	18
Devonwood	1776	459	2235	8334	27
Eaton	139,563	0	139,563	1,179,209	12
Gooseberry	9363	0	9363	25,886	36
Kinneloa East	13,524	1671	15,195	27,524	55
Kinneloa West	15,776	0	15,776	26,759	59
Lannan	11,674	1743	13,417	31,653	42
Las Flores	22,562	0	22,562	41,898	54
Rubio	26,201	9221	35,422	113,185	31
Sierra Madre D	56,253	2699	58,952	104,285	57
Sunnyside	1381	0	1381	3823	36

We estimate observed volume change from the DEM differencing between January 20 airborne lidar surveys (NV5 et al. 2025) and February 23 UAV lidar surveys. Excavated volume is measured and reported by the Los Angeles County Department of Public Works based on truck loads of debris removed from the basins between the airborne and UAV surveys. Deposited volume represents the total sediment yield in the debris basins by adding the observational volume change and the excavated volume. We calculate the design capacity loss using the deposited volume and debris basin design capacity, which is publicly available from Los Angeles County Department of Public Works (2021)

Figure 9 compares the measured debris volumes in 14 debris basins with the volumes predicted by the USGS empirical regression model for the February 13, 2025 storm event. The left panel (a) presents the comparison in linear space, and the right panel (b) shows the same data on a logarithmic scale. The model shows better performance in smaller basins, and tends to overpredict debris volumes in basins with larger drainage areas.

Measuring post-fire dry-ravel accumulation in channels

To evaluate the contribution of dry-ravel loading to debris flows, we performed DEM differencing to measure sediment accumulation in channel networks following the Eaton Fire. Figure 10 presents both the post-fire and post-storm DEM differencing

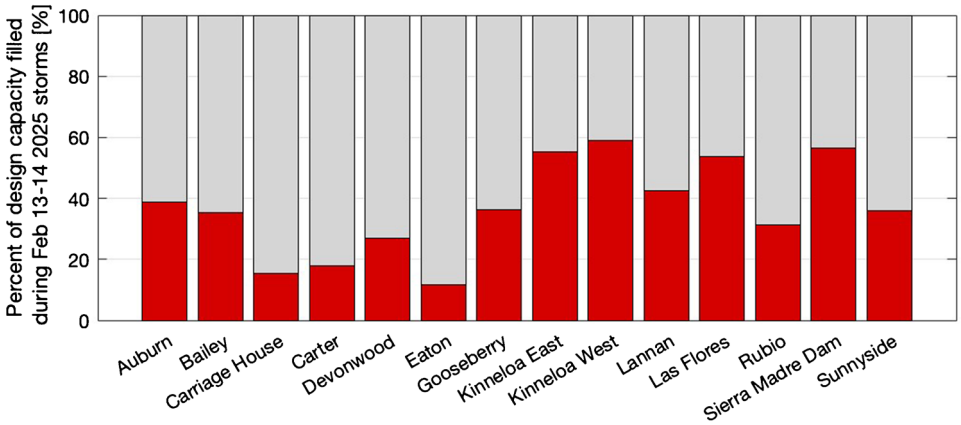

Fig. 8 Estimated debris volumes delivered to each basin during the February 13 storm event, plotted as a percentage of each basin's total design capacity (Los Angeles County Department of Public Works 2021)

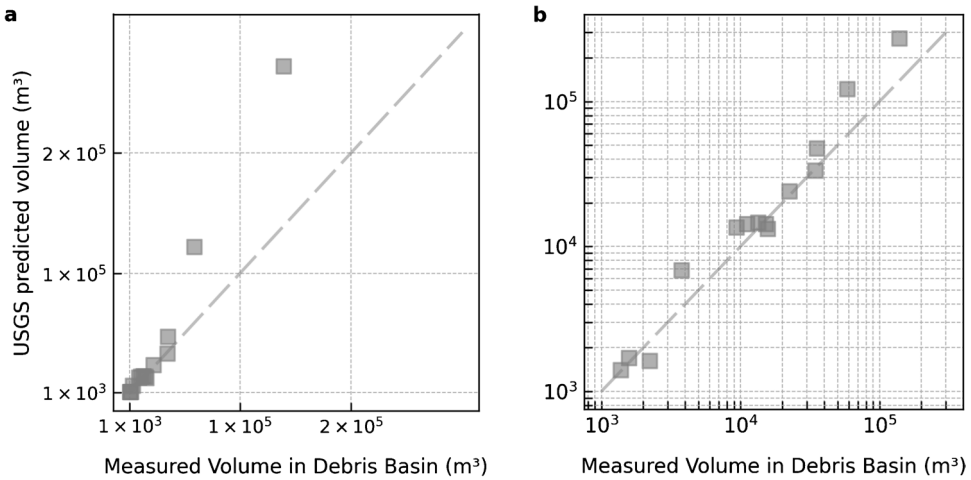

Fig. 9 Comparison of measured debris basin sediment yields with USGS predictions for the February 13 storm event. The data are shown in linear space in **a** and logarithmic space in **b**

results. The post-fire DEM differencing reveals substantial sediment accumulation within the channel networks, supporting the dry-ravel hypothesis (Lamb et al. 2011; DiBiase and Lamb 2020). Figure 10b illustrates how, during the storm event, the sediment lining the channel networks was subsequently evacuated and transported downstream into the debris basins.

We used DEM differencing results to estimate post-fire sediment loading (dry ravel) and post-storm sediment removal within the channel networks. In Fig. 11, we compared the (i) post-fire sediment loading, (ii) post-storm sediment removal, and (iii) USGS-estimated sediment yield with the measured sediment volume in debris basins. From the debris basin sediment yield, we calculated soil losses of 256.5, 257.3, 316.9, 157.4, and 254.7 tons per hectare for the Bailey, Carriage House, Sunnyside, Carter, and Auburn basins, respectively (DiBiase and Lamb 2013). We find that all three inputs (i)–(iii) are strong linear predictors of the measured sediment volumes in the debris basins. We fit the data with a simple model of the form $y = ax$, where y is the measured sediment volume in the debris basin and x is the input variable (Fig. 11). Among the three regressions, post-storm sediment removal exhibited a slope (a) closest to 1. This comparison between post-storm sediment removal and debris basin sediment yield indicates that virtually all of the sediment mobilized in the debris flows originated from within the channel network, with minimal contribution from surrounding hillslopes. Finally, in contrast to USGS models, which rely on rainfall intensity data, our UAV-based method requires no such input, enabling sediment hazard prediction prior to rainfall events.

Using our UAV-based differencing approach, we can quantify the difference between post-fire channel loading and post-storm sediment removal, which represents the volume of sediment left behind after the storm. This residual material remains primed to be mobilized in subsequent storms, so quantifying its volume allows us to estimate future hazard potential relative to remaining debris basin capacities. Although a second storm may not mobilize as much sediment as the first, the reduced capacity of debris basins could result in a higher downstream hazard. In the case of the catchment draining to the Bailey debris basin, approximately 23% of dry-ravel material has yet to be cleared out (Fig. 11).

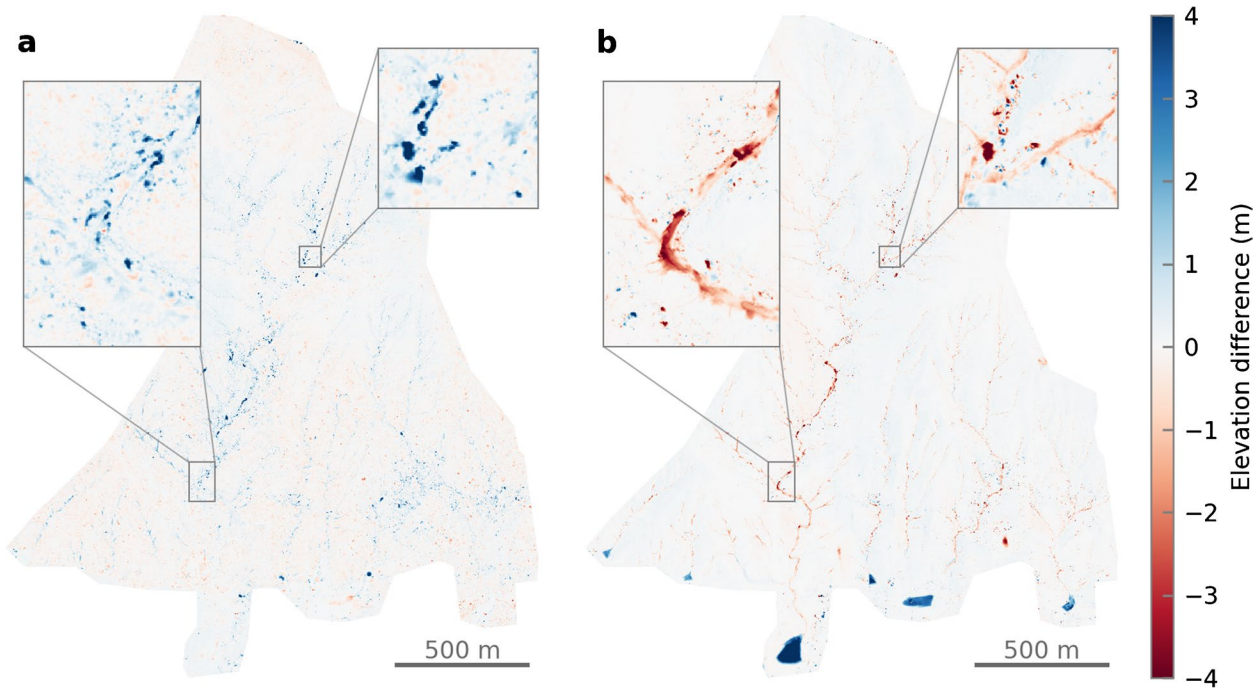

Fig. 10 Elevation differencing maps of the Bailey catchments. **a** Post-fire DEM differencing between UAV lidar collected on February 10, 2025, and pre-fire USGS airborne lidar collected in 2023 (U.S. Geological Survey 2023). **b** Post-storm DEM differencing between UAV lidar surveys collected on February 19 and February 10, 2025. The colorbar is clipped to ±4 *m* for visualization

Our observation of the post-storm sediment removal from the channel network exceeding the measured debris basin volumes (Fig. 11) likely reflects the measurement uncertainties of the UAV lidar and DEM differencing workflow. Additionally, this discrepancy may stem from differences in sediment compaction. Before the storm, sediment stored in the ravel cones lining the channel network may have exhibited higher porosity because of the relatively homogeneous grain size and poor grain packing. In contrast, sediment deposited in debris basins may be less porous due to the poorly-sorted admixture of grain sizes (e.g., sand and mud particles filling the spaces between gravel), resulting in a smaller measured volume despite a similar sediment mass.

Discussion

Implications for predicting post-fire debris-flow hazards

Our observations indicate that the sediment mobilized as dry ravel during and immediately following the Eaton Fire can explain the majority of the sediment volume transported out of the catchment during the debris-flow-producing rainstorm (Fig. 11). In other words, measured volumes of dry-ravel deposits may serve as a useful, data-driven predictor of upcoming debris-flow volumes. However, there are a number of important caveats of this approach.

First, our observations come from a single fire-flood cycle in a landscape that has been identified as having a particularly strong dry-ravel response following wildfire (Lamb et al. 2011; DiBiase and Lamb 2013). Many other post-fire landscapes experience limited sediment mobilization via dry ravel (Raymond et al. 2020; McGuire and Youberg 2020). In these settings, debris flows may be caused more from syn-rainstorm entrainment of hillslope soils rather than the destabilization and collapse of the ravel deposits filling channels (McGuire et al. 2017; Alessio et al. 2021; Dunne et al. 2025).

Second, redistribution and transient storage of sediment within the catchment may modulate the size of the observed debris flows in the first major rainstorm following fire (Yanites et al. 2025). For example, the long, low-gradient trunk channels in large catchments may serve as sediment capacitors that aggrade with sediment during the first post-fire rainstorm (when sediment is exported out of the steeper, first- and second-order catchments as debris flows). Then, subsequent rainstorms may mobilize sediment from the low-gradient channels and export it to the terminal debris basins. Thus, we expect catchment size and channel network topology to modulate the relationships shown in Fig. 11 between post-fire sediment loading and post-rainstorm sediment removal.

Using UAV lidar for debris-flow hazard assessment

UAV lidar systems offer a low-cost, high-resolution, and agile approach to rapid postfire debris-flow hazard assessment. In contrast to traditional airborne lidar, which is constrained by cost, flight logistics, and restricted airspace, UAV platforms can be rapidly deployed and operated at finer spatial and temporal resolutions (Kellner et al. 2019). For the Eaton Fire, whereas airborne lidar surveys were conducted on January 20–21 and February 20, 2025,

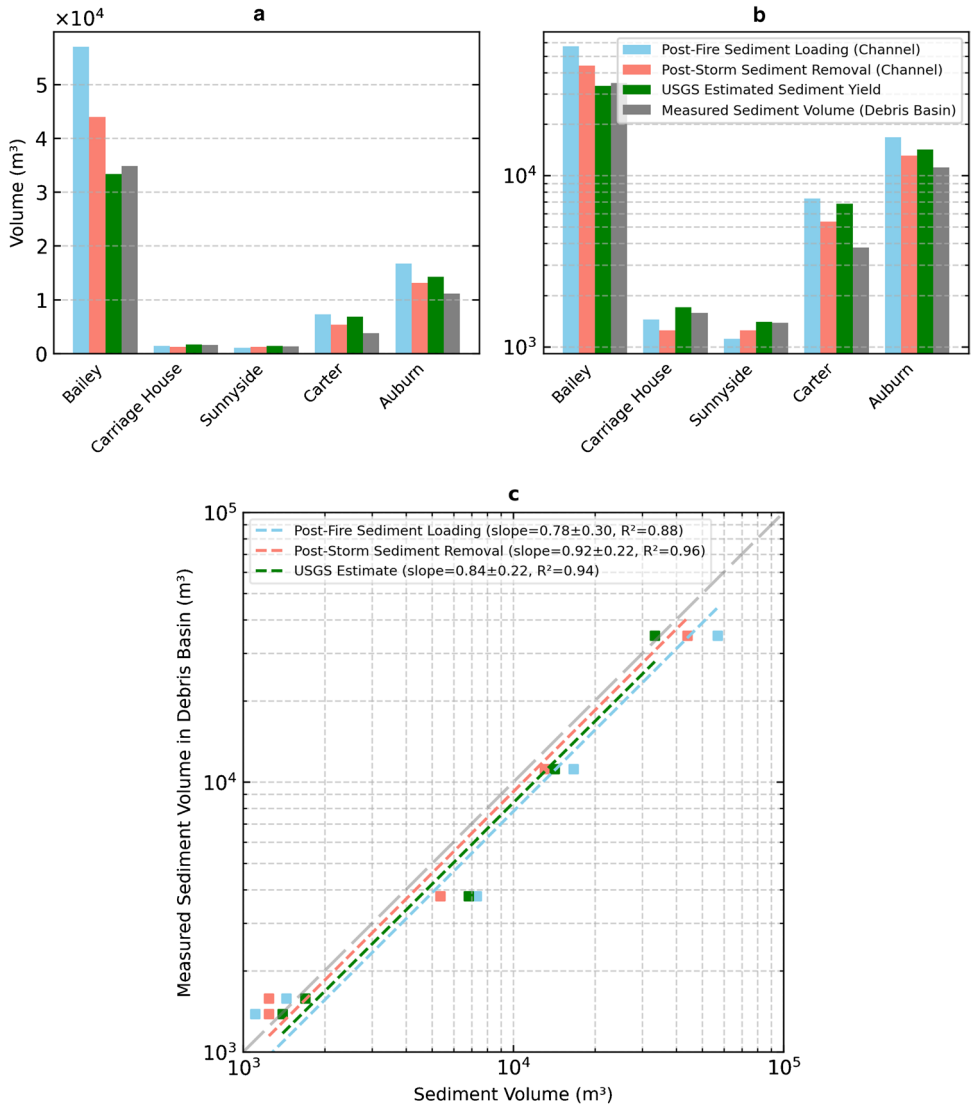

Fig. 11 A comparison between the (i) pre-storm sediment loading in the channel networks, (ii) post-storm erosion of sediment from the channel networks, (iii) predicted debris-flow volumes based on the USGS model, and (iv) observed debris-flow volumes based on the sediment deposition in debris basins. The sediment volumes were measured across five debris basins (Bailey, Carriage House, Sunnyside, Carter, and Auburn; Fig. 1). The same data are shown using a linear scale in **a** and a logarithmic scale in **b**. Dashed lines in **c** denote linear regressions constrained to pass through the origin, calculated by minimizing the sum of squared differences between log(x) and log(y). Model fit statistics include the slope and the coefficient of determination (R^2)

we conducted UAV lidar surveys on ten separate dates across key debris basins and the Bailey catchments, capturing geomorphic changes before and after each rain event. While airborne lidar provides broader spatial coverage (NV5 et al. 2025), UAV lidar can serve a complementary role by guiding the optimal timing of more costly airborne data acquisitions. For example, our UAV surveys on February 14, 19, and 23 revealed that sediment volume estimates made immediately after the February 14 storm overestimated deposition by approximately 15% due to ponded water. By the time of the February 20 airborne lidar survey, the basins had largely drained, with only 0–5% excess water. Such findings underscore the importance of repeated high-resolution surveys to distinguish transient signals (e.g., ponded water) that may confound geomorphic interpretations if captured in a single airborne snapshot.

Additionally, UAV lidar systems equipped with high-resolution RGB cameras enable simultaneous collection of true-color imagery, allowing for the generation of colorized point clouds and orthomosaics (e.g., Fig. 3a). These products provide critical visual context for hazard assessment (Román et al. 2025), such as identifying transported boulders, woody debris, and potential infrastructure damage that may be missed in airborne lidar datasets. As UAV lidar technology continues to improve in resolution, payload, and autonomy, its integration into regional hazard monitoring frameworks

will not only enhance postfire response but also improve the strategic deployment of airborne lidar resources (Chen et al. 2025).

Using UAV lidar for hazard prediction and mitigation

The UAV lidar system demonstrated powerful capabilities for advancing postfire hazard mitigation. An important outcome of our surveys was the ability to measure dry-ravel sediment accumulations in channels immediately after fire and prior to any rainfall (Palucis et al. 2021). In steep, bedrock-dominated landscapes, where sediment supply in channels is a key control on debris-flow initiation (Lamb et al. 2011, 2013; DiBiase and Lamb 2013, 2020), postfire sediment yield estimation is essential for forecasting sediment transport during subsequent storm events. Unlike existing empirical models, which require storm-specific rainfall inputs (Gartner et al. 2014), UAV lidar enables direct quantification of sediment stockpiles before precipitation occurs, establishing a data-driven route to forecasting debris-flow hazard in advance of rainfall. This capability marks a potential paradigm shift in debris-flow prediction in steep landscapes such as the SGM, allowing for preemptive hazard prediction and response planning.

The advantages of UAV lidar surveys extend beyond immediate response. First, they enable tracking of cumulative basin fill over the course of a storm season, with each survey serving as a baseline for subsequent events. Second, the data provide valuable feedback for model validation: measured sediment volumes can be compared to model predictions, allowing calibration of empirical relationships (Gartner et al. 2014). Third, the residual material, calculated as the difference between post-fire channel loading and post-storm sediment removal, represents mobilizable sediment that remains within the channel network and can be used to estimate potential mobilized sediment volumes during the next storm. Together, these capabilities position UAV lidar as a transformative tool for both quantitative analysis and operational decision-making in postfire debris-flow hazard management.

In addition to sediment supply estimation, UAV lidar proved highly effective for storm-scale assessment of debris basin fill and remaining capacity following storm events. Traditionally, estimating debris volumes requires manual inspections or ground-based (e.g., total station) surveys, which are time-consuming and in some cases unsafe because of ongoing debris basin excavation. In the Eaton Fire response, our UAV lidar surveys provided actionable information to hazard managers, prioritizing debris basin excavation. Second, our surveys offered a rare opportunity to ground-truth the performance of postfire debris-flow models using real event data.

Logistical challenges and opportunities

Despite the advances in UAV lidar, our deployment also exposed several operational challenges and constraints that must be navigated to make this technology a routine part of hazard management. Airspace access is a primary concern. Postfire landscapes often are subject to Temporary Flight Restrictions during and immediately after wildfires, to avoid interfering with firefighting aircrafts (Kang et al. 2024; Keerthinathan et al. 2023). In our case, we had to closely coordinate with the Federal Aviation Administration to gain clearance once the active firefighting had ceased. Additional logistical coordination with emergency responders and public works crews, such as the U.S. Forest Service (USFS) and Los Angeles County, was essential to obtain permission for UAV surveys without interfering with ongoing excavation activities. We recommend early engagement with the regulatory agencies to secure rapid access windows for UAV surveys as soon as conditions allow. Weather, particularly low clouds, is another factor that can limit UAV GPS signals and or constrain lidar capability (Dreissig et al. 2023). For example, on February 14, 2025, one day after the storm event, low clouds over the high-elevation and steep terrain of the Bailey catchments disrupted GPS reception and constrained lidar performance.

Our experience with the Eaton Fire suggests several strategic steps to fully integrate UAV lidar into routine postfire debris-flow hazard management. First, stakeholders should treat UAV lidar as a standard component of the postfire toolkit, alongside timelapse camera stations, rain gauges, and field inspections. Remote camera deployment in particular is a low-cost complement. These cameras, networked where possible for real-time viewing, provided immediate confirmation of flow occurrence and helped interpret the lidar-detected changes. The combination of continuous visual monitoring and periodic lidar surveys creates a robust observational framework: cameras flag when and where events happen, and UAV lidar quantifies the consequences.

Conclusions

Our study demonstrates that UAV lidar provides a powerful and agile tool for rapid assessment and prediction of postfire debris flows. Using the Eaton Fire as a case study, we show that UAV lidar surveys can effectively capture both post-storm sediment deposition in debris basins and post-fire sediment loading (dry-ravel deposits) in channel networks. The ability to quantify sediment deposition immediately after individual rainfall events offers critical insights into how quickly basin capacity is reduced. This timely information supports more informed decisions about excavation priorities and serves as a valuable reference for calibrating and validating empirical models, offering direct measurements that improve the accuracy of volume predictions. Post-fire dry-ravel sediment loading provides a rare opportunity to measure sediment supply in channels before rainfall occurs. Both post-fire sediment loading and post-storm sediment removal show strong linear correlation with measured debris basin volumes, indicating that nearly all mobilized debris originated from within the channel network. Unlike traditional USGS models that rely on rainfall inputs, the UAV-based method enables sediment hazard prediction even before rain events. Additionally, the comparison between pre- and post-storm surveys allows for quantification of residual sediment remaining in the channels, which represents future hazard potential. Approximately 23% of dry-ravel material remained unmobilized after the first storm and could pose a risk in subsequent storms, particularly given the reduced capacity of debris basins. As a result, UAV lidar shifts debris-flow prediction from reactive to anticipatory, improving both the accuracy and timeliness of postfire hazard management.

While UAV lidar provides significant advantages, its successful integration into postfire hazard workflows requires coordination with regulatory agencies and emergency responders, as well as

favorable weather conditions. Airspace access, cloud cover, and field logistics must be carefully managed. Nevertheless, our experience shows that early planning and collaboration can enable timely deployments that maximize scientific and operational value. We recommend that UAV lidar become a routine component of postfire hazard mitigation efforts, particularly in high-risk terrain where rapid sediment mobilization is likely. When combined with rainfall monitoring, timelapse cameras, and empirical modeling, UAV lidar enhances our ability to observe, predict, and respond to debris-flow hazards in a data-driven and efficient manner. As lidar platforms continue to improve, their integration into multi-sensor hazard assessment frameworks will be key to protecting communities in an era of increasing wildfire and extreme weather events.

Acknowledgements

Thank you to Pete Robichaud, Jonathan Yonni Schwartz, and Miranda Beasley at the US Forest Service (USFS) for help with field access, field safety, and permitting (USFS Special Use Permit: Authorization ID LAR106004). Thank you to Iraj Nasseri, Ken Zimmer, Dai Bui, Armando D'Angelo, and other staff at Los Angeles County Public Works (LACPW) for debris-basin access and sharing information about debris basin clean-outs. Thank you to Vincent Doud, Steven Chaffin, and Tanner Aunan for processing the FAA authorization and granting permission to conduct UAV operations in the restricted airspace. Our work benefited from planning discussions with Don Lindsay and Jason Kean, and the postfire response teams at the California Geological Survey and the U.S. Geological Survey. This project was supported by donors to the Eaton Fire Research Fund at Caltech. UAV was funded by the Caltech Center for Autonomous Systems and Technologies (CAST). We thank Dev Dalmia, Harrison Martin, and Justin Nghiem for helping with field surveys. E. Geyman acknowledges support from the National Science Foundation Graduate Research Fellowship Program (GRFP) and the Fannie and John Hertz Foundation. Z. Chen acknowledges support from Katherine Scharer and Devin McPhillips of the U.S. Geological Survey.

Funding

This project was funded by the Eaton Fire Research Fund at Caltech.

Data availability

The datasets used during this study are available from the corresponding author upon reasonable request and subject to approval from the relevant agencies.

Code availability

The custom scripts developed for data processing and analysis are available from the corresponding author via email.

Declarations

Competing interests The authors declare no competing interests.

Appendix. Debris basin coordinates

Table 3 Coordinates of the 14 debris basins surveyed in this study

Debris basin	UTM easting	UTM northing
Auburn	402,628	3,781,985
Bailey	402,170	3,781,770
Carriage House	401,459	3,782,180
Carter	403,230	3,781,969
Eaton Wash	391,724	3,783,525
Devonwood	395,770	3,785,730
Gooseberry	396,794	3,784,182
Kinneloa East	400,139	3,782,993
Kinneloa West	399,959	3,783,044
Lannan	404,809	3,781,773
Las Flores	396,182	3,785,103
Rubio	396,579	3,784,882
Sierra Madre Dam	403,899	3,782,179
Sunnyside	401,777	3,782,085

Coordinates are reported in WGS84 UTM zone 11N

References

ALERTCalifornia (2025) University of California San Diego. https://alertcalifornia.org/, accessed: 2025-07-11

Alessio P, Dunne T, Morell K (2021) Post-wildfire generation of debris-flow slurry by rill erosion on colluvial hillslopes. J Geophys Res Earth Surf 126(11):e2021JF006108

Besl P, McKay ND (1992) A method for registration of 3-D shapes. IEEE Trans Pattern Anal Mach Intell 14(2):239–256. https://doi.org/10.1109/34.121791

Butler H, Chambers B, Hartzell P et al (2021) PDAL: an open source library for the processing and analysis of point clouds. Comput Geosci. https://doi.org/10.1016/j.cageo.2020.104680

Cannon SH, DeGraff J (2009) The increasing wildfire and post-fire debris-flow threat in western USA, and implications for consequences of climate change. In: Sassa K, Canuti P (eds) Landslides – Disaster Risk Reduction. Springer, pp 177–190. https://doi.org/10.007/978-3-540-69970-5_9

Cannon SH, Gartner JE, Parrett C et al (2003) Wildfire-related debris-flow generation through episodic progressive sediment-bulking processes, western USA. In: Debris-Flow Hazards and Related Phenomena, pp 71–82. https://pubs.usgs.gov/publication/70025321

Chen B, Maurer J, Gong W (2025) Applications of UAV in landslide research: a review: B. chen et al. Landslides pp 1–20. https://doi.org/10.1007/s10346-025-02547-2

Chen Z, Gao B, Devereux B (2017) State-of-the-art: DTM generation using airborne lidar data. Sensors 17(1):150. https://doi.org/10.3390/s17010150

Conrad O, Bechtel B, Bock M et al (2015) System for automated geoscientific analyses (SAGA) v. 2.1.4. Geosci Model Dev 8(7):1991–2007. https://doi.org/10.5194/gmd-8-1991-2015

DiBiase RA, Lamb MP (2013) Vegetation and wildfire controls on sediment yield in bedrock landscapes. Geophys Res Lett 40(6):1093–1097. https://doi.org/10.1002/grl.50277

DiBiase RA, Lamb MP (2020) Dry sediment loading of headwater channels fuels post-wildfire debris flows in bedrock landscapes. Geology 48(2):189–193. https://doi.org/10.1130/G46847.1

Dreissig M, Scheuble D, Piewak F et al (2023) Survey on lidar perception in adverse weather conditions. In: 2023 IEEE Intelligent vehicles symposium (IV), pp 1–8. https://doi.org/10.1109/IV55152.2023.10186539

Dunne T, Alessio P, Morell KD (2025) Recruitment and dispersal of post-wildfire debris flows. J Geophys Res Earth Surf 130(7):e2025JF008325

Eaton EC (1936) Flood and erosion control problems and their solution. Trans Am Soc Civ Eng 101(1):1302–1330. https://doi.org/10.1061/TACEAT.0004726

Florsheim JL, Keller EA, Best DW (1991) Fluvial sediment transport in response to moderate storm flows following chaparral wildfire, Ventura County, Southern California. Geol Soc Am Bull 103(4):504–511

Freeman TG (1991) Calculating catchment area with divergent flow based on a regular grid. Comput Geosci 17(3):413–422. https://doi.org/10.1016/0098-3004(91)90048-I

Gabet EJ (2003) Sediment transport by dry ravel. J Geophys Res Solid Earth. https://doi.org/10.1029/2001JB001686

Gartner JE, Cannon SH, Santi PM (2014) Empirical models for predicting volumes of sediment deposited by debris flows and sediment-laden floods in the transverse ranges of Southern California. Eng Geol 176(24):45–56. https://doi.org/10.1016/j.enggeo.2014.04.008

Graber AP, Thomas MA, Kean JW (2023) How long do runoff-generated debris-flow hazards persist after wildfire? Geophys Res Lett 50(19):e2023GL105101. https://doi.org/10.1029/2023GL105101

Heimsath AM, DiBiase RA, Whipple KX (2012) Soil production limits and the transition to bedrock-dominated landscapes. Nat Geosci 5(3):210–214. https://doi.org/10.1038/ngeo1380

Hubbert KR, Wohlgemuth PM, Beyers JL et al (2012) Post-fire soil water repellency, hydrologic response, and sediment yield compared between grass-converted and chaparral watersheds. Fire Ecol 8(2):143–162. https://doi.org/10.4996/fireecology.0802143

Kang DK, Fischer E, Olsen MJ et al (2024) Optimising disaster response: opportunities and challenges with uncrewed aircraft system (UAS) technology in response to the 2020 labour day wildfires in Oregon, USA. Int J Wildland Fire. https://doi.org/10.1071/WF23089

Keerthinathan P, Amarasingam N, Hamilton G et al (2023) Exploring unmanned aerial systems operations in wildfire management: data types, processing algorithms and navigation. Int J Remote Sens 44(18):5628–5685. https://doi.org/10.1080/01431161.2023.2249604

Kellner JR, Armston J, Birrer M et al (2019) New opportunities for forest remote sensing through ultra-high-density drone lidar. Surv Geophys 40(4):959–977. https://doi.org/10.1007/s10712-019-09529-9

Krammes JS (1965) Seasonal debris movement from steep mountain slide slopes in Southern California. USDA MISC PUB 979(1965):85–89

Lague D, Brodu N, Leroux J (2013) Accurate 3D comparison of complex topography with terrestrial laser scanner: application to the Rangitikei canyon (N-Z). ISPRS J Photogramm Remote Sens 82:10–26. https://doi.org/10.1016/j.isprsjprs.2013.04.009

Lamb MP, Scheingross JS, Amidon WH et al (2011) A model for fire-induced sediment yield by dry ravel in steep landscapes. J Geophys Res. https://doi.org/10.1029/2010JF001878

Lamb MP, Levina M, DiBiase RA et al (2013) Sediment storage by vegetation in steep bedrock landscapes: theory, experiments, and implications for postfire sediment yield. J Geophys Res Earth Surf 118(2):1147–1160. https://doi.org/10.1002/jgrf.20058

Los Angeles County Coordinated Joint Information Center (2025) Media update: Eaton and Palisades fires 1/24/25. https://recovery.lacounty.gov/2025/01/24/media-update-eaton-and-palisades-fires-1-24-25/, accessed: 2025-08-01

Los Angeles County Department of Public Works (2021) Hydrologic report 2020–2021. https://dpw.lacounty.gov/wrd/report/acrobat/Hydrologic%20Report%202020-2021.pdf, accessed: 2025-08-01

Los Angeles County Department of Public Works (2025) Rainfall data [dataset]. https://dpw.lacounty.gov/wrd/rainfall, accessed: 2025-08-01

McGuire LA, Youberg AM (2020) What drives spatial variability in rainfall intensity-duration thresholds for post-wildfire debris flows? Insights from the 2018 Buzzard Fire, NM, USA. Landslides 17(10):2385–2399

McGuire LA, Rengers FK, Kean JW et al (2017) Debris flow initiation by runoff in a recently burned basin: is grain-by-grain sediment bulking or en masse failure to blame? Geophys Res Lett 44(14):7310–7319

Murchek JT, Drenth BJ, Reitman JJ et al (2025) The feasibility of using lidar-derived digital elevation models for gravity data reduction. Tech. rep., US Geological Survey, https://pubs.usgs.gov/publication/ofr20251019

Nikolopoulos E, Borga M, Creutin J et al (2015) Estimation of debris flow triggering rainfall: influence of rain gauge density and interpolation methods. Geomorphology 243:40–50. https://doi.org/10.1016/j.geomorph.2015.04.028

NV5, University of California-San Diego, United States Geological Survey (2025) Preliminary digital elevation models for Eaton Fire, CA 2025 [dataset]. https://doi.org/10.5069/G9JH3JD6, openTopography, Accessed: 2025-08-01

Palucis MC, Ulizio TP, Lamb MP (2021) Debris flow initiation from ravel-filled channel bed failure following wildfire in a bedrock landscape with limited sediment supply. GSA Bull 133(9):2079–2096. https://doi.org/10.1130/B35822.1

Peduto D, Iervolino L, Esposito G et al (2022) Clues of wildfire-induced geotechnical changes in volcanic soils affected by post-fire slope instabilities. Bull Eng Geol Environ 81(10):454. https://doi.org/10.1007/s10064-022-02947-x

Peucker TK, Douglas DH (1975) Detection of surface-specific points by local parallel processing of discrete terrain elevation data. Comput Graph Image Process 4(4):375–387. https://doi.org/10.1016/0146-664X(75)90005-2

Pingel TJ, Clarke KC, McBride WA (2013) An improved simple morphological filter for the terrain classification of airborne LIDAR data. ISPRS J Photogramm Remote Sens 77:21–30. https://doi.org/10.1016/j.isprsjprs.2012.12.002

Prancevic JP, Lamb MP, Fuller BM (2014) Incipient sediment motion across the river to debris-flow transition. Geology 42(3):191–194. https://doi.org/10.1130/G34927.1

Ramirez RA, Jang W, Kwon TH (2024) Wildfire burn severity and post-wildfire time impact mechanical and hydraulic properties of forest soils. Geoderma Reg 39:e00856. https://doi.org/10.1016/j.geodrs.2024.e00856

Raymond CA, McGuire LA, Youberg AM et al (2020) Thresholds for post-wildfire debris flows: insights from the Pinal Fire, Arizona, USA. Earth Surf Process Landforms 45(6):1349–1360

Rengers FK, McGuire LA, Kean JW et al (2021) Movement of sediment through a burned landscape: sediment volume observations and model comparisons in the San Gabriel Mountains, California, USA. J Geophys Res Earth Surf 126(7):e2020JF006053. https://doi.org/10.1029/2020JF006053

Rengers FK, Bower S, Knapp A et al (2024) Evaluating post-wildfire debris-flow rainfall thresholds and volume models at the 2020 Grizzly Creek Fire in Glenwood Canyon, Colorado, USA. Nat Hazards Earth Syst Sci 24(6):2093–2114. https://doi.org/10.5194/nhess-24-2093-2024

Rice RM (1982) Sedimentation in the chaparral: how do you handle unusual events? In: Sediment budgets and routing in forested drainage basins: Proceedings of the symposium; 31 May - 1 June 1982; Corvallis, Oregon Gen Tech Rep PNW-141 Portland, Oregon: Pacific Northwest Forest and Range Experiment Station, Forest Service, US Department of Agriculture; 1982: 39-49 https://research.fs.usda.gov/treesearch/8548

Román A, Tovar-Sánchez A, Larrad M et al (2025) UAV imagery in natural disasters: real-time damage assessment of flash flooding events. Ecol Inform 103433. https://doi.org/10.1016/j.ecoinf.2025.103433

Scheidl C, Rickenmann D, Chiari M (2008) The use of airborne LiDAR data for the analysis of debris flow events in Switzerland. Nat Hazards Earth Syst Sci 8(5):1113–1127. https://doi.org/10.5194/nhess-8-1113-2008
Shepard D (1968) A two-dimensional interpolation function for irregularly-spaced data. In: Proceedings of the 1968 23rd ACM national conference. Association for Computing Machinery, ACM '68, pp 517–524, https://doi.org/10.1145/800186.810616
Staley DM, Wasklewicz TA, Kean JW (2014) Characterizing the primary material sources and dominant erosional processes for post-fire debris-flow initiation in a headwater basin using multi-temporal terrestrial laser scanning data. Geomorphology 214:324–338. https://doi.org/10.1016/j.geomorph.2014.02.015
Staley DM, Negri JA, Kean JW et al (2016). Updated logistic regression equations for the calculation of post-fire debris-flow likelihood in the western United States. https://doi.org/10.3133/ofr20161106
Staley DM, Negri JA, Kean JW et al (2017) Prediction of spatially explicit rainfall intensity–duration thresholds for post-fire debris-flow generation in the western United States. Geomorphology 278:149–162. https://doi.org/10.1016/j.geomorph.2016.10.019
Tarboton DG, Bras RL, Rodriguez-Iturbe I (1991) On the extraction of channel networks from digital elevation data. Hydrol Process 5(1):81–100. https://doi.org/10.1002/hyp.3360050107
U.S. Geological Survey (2018) The scientific background information for emergency assessment of postfire debris-flow hazards. https://www.usgs.gov/programs/landslide-hazards/science/scientific-background, accessed: 2025-08-01
U.S. Geological Survey (2020) Lidar base specification tables. https://www.usgs.gov/ngp-standards-and-specifications/lidar-base-specification-tables, accessed 2025-12-04
U.S. Geological Survey (2023) United States geological survey 3d elevation program 1 meter digital elevation model. https://doi.org/10.5069/G9NP22NT, distributed by OpenTopography. Accessed 2025-12-04
U.S. Geological Survey (2025) USGS post-fire debris-flow hazard assessment. ArcGIS Dashboards, https://usgs.maps.arcgis.com/apps/dashboards/c09fa874362e48a9afe79432f2efe6fe, accessed: 2025-08-01
Wang L, Liu H (2006) An efficient method for identifying and filling surface depressions in digital elevation models for hydrologic analysis and modelling. Int J Geogr Inf Sci 20(2):193–213. https://doi.org/10.1080/13658810500433453
Yanites BJ, Clark MK, Roering JJ et al (2025) Cascading land surface hazards as a nexus in the Earth system. Science 388(6754):eadp9559

Zhiang Chen · Emily C. Geyman · Michael P. Lamb (✉)
Division of Geological and Planetary Sciences, California Institute of Technology, 1200 E California Blvd, Pasadena, CA 91125, USA
Email: mpl@caltech.edu

Zhiang Chen
Email: zhiang.chen@caltech.edu

Emily C. Geyman
Email: egeyman@caltech.edu